On the Design of Expressive and Trainable Pulse-based Quantum Machine Learning Models

Han-Xiao Tao, Xin Wang, and Re-Bing Wu

Center for Intelligent and Networked Systems, Department of Automation, Tsinghua University, Beijing, 100084, China

Pulse-based Quantum Machine Learning (QML) has emerged as a novel paradigm in quantum artificial intelligence due to its exceptional hardware efficiency. For practical applications, pulse-based models must be both expressive and trainable. Previous studies suggest that pulse-based models under dynamic symmetry can be effectively trained, thanks to a favorable loss landscape that has no barren plateaus. However, the resulting uncontrollability may compromise expressivity when the model is inadequately designed. This paper investigates the requirements for pulse-based QML models to be expressive while preserving trainability. We present a necessary condition pertaining to the system's initial state, the measurement observable, and the underlying dynamical symmetry Lie algebra, supported by numerical simulations. Our findings establish a framework for designing practical pulse-based QML models that balance expressivity and trainability.

1 INTRODUCTION

Quantum computing holds substantial promise for significantly improving the efficiency of both training and inference in machine learning tasks [1, 2, 3, 4]. However, in the noisy intermediate-scale quantum (NISQ) era, the lack of error correction necessitates that quantum machine learning (QML) collaborates with classical computers [5, 6] through variational quantum models. In this framework, quantum models execute the inference task, while the classical computer manages the training.

In the literature, variational QML models predominantly employ gate-based parameterized quantum circuits, also known as quantum neural networks (QNNs) [7, 8]. Since all gates are ultimately implemented through control pulses on the relevant physical qubits, recent proposals suggest that QML models may be parameterized directly by these continuous-time control pulses instead of discrete-time gate parameters [9, 10, 11, 12, 13, 14, 15, 16]. In contrast to gate-based models, pulse-based models are grounded in physical systems without abstraction, making them more accessible to engineers due to their straightforwardness and hardware efficiency [17, 18, 19, 20, 21].

In principle, within the finite coherence time, pulse-based QML models are more expressive compared to their gate-based counterparts because they function as "infinitely" deep data-re-uploading QNNs [22]. This advantage has been demonstrated in our previous study [22], where we also proved that pulse-based models achieve full expressivity (i.e., the ability to approximate arbitrary functions [23, 24, 25, 26]) when the underlying quantum system is ensemble controllable. This criterion provides a control-oriented framework for designing pulse-based models, analogous to the design of universal quantum computers [27]. Nonetheless, in systems comprising a large number of qubits, the requirement for controllability becomes excessively stringent as it inevitably leads to barren plateaus within the loss landscape [28, 29]. This phenomenon results in an exponential de-

Re-Bing Wu: rbwu@tsinghua.edu.cn

cay of loss gradients (or, equivalently, the loss variance [30, 31]) in the asymptotic temporal limit [32] and the large qubit-number limit, thus rendering optimization within large-scale systems impracticable [8, 33, 34, 35, 36, 37, 38]. A similar trade-off between expressivity and trainability is observed in gate-based models, where the loss function predominantly concentrates as the circuit attains greater expressivity [33, 39, 40].

To alleviate the conflict between expressivity and trainability, controllability must be sacrificed in the design of pulse-based models. Larocca *et al.* [28] reveals that trainability is contingent on the degree of controllability characterized by the size and symmetry of its dynamical Lie algebra. The findings indicate that a symmetry-restricted model has the potential to circumvent barren plateaus, thus providing a practical diagnostic approach for the design of QML models. Building upon this insight, a Lie-algebraic theory for barren plateaus has been developed, based on which an exact variance formula is derived for the loss function. It is demonstrated that the variance scales inversely with the dimension of the dynamical Lie algebra, provided that either the initial state or observable is contained within the Lie algebra [41, 42]. Diaz *et al.* [43] extends beyond the Lie-algebraic framework by analyzing parameterized matchgate circuits. By decomposing the operator space into Lie group modules, they derive an exact variance formula for loss functions applicable to arbitrary initial states and observables, demonstrating that barren plateaus can emerge from generalized global operators and are dependent on module dimensions rather than solely on the dimension of the dynamical Lie algebra.

The existing literature provides a Lie algebraic framework for evaluating the trainability of uncontrollable pulse-based QML models induced by dynamic symmetry, but the expressivity of these models remains ambiguous. In the present study, we demonstrate that an ill-suited selection of either the initial state or the measurement observable can result in the loss of expressivity, and conduct a sys-

tematic analysis on the expressivity of pulse-based QML models within the context of dynamic symmetry. In contrast to the Fourier-series analysis typically used to assess the expressivity of data-reuploading gate-based models [44, 45, 46, 47, 48], we utilize the polynomial expansion of nonlinear functions epitomized by the pulse-based model based on Dyson-series analysis (also known as Fliess-series in control theory for input-output analysis of nonlinear systems [49]). This analysis yields a Lie algebraic tool for the design of expressive pulse-based models with dynamic symmetry.

The structure of the paper is as follows: Section 2 introduces essential background on pulse-based QML models and the existing results on the trainability under dynamic symmetry. Section 3 analyzes the expressivity of pulse-based models through the Dyson-series expansion from which a necessary condition is derived. In Section 4, numerical experiments are conducted to demonstrate the expressivity of pulse-based models with dynamic symmetry, and the balance between expressivity and trainability. Finally, Section 5 draws the conclusion and future perspectives.

2 PULSE-BASED QML MODELS with dynamical symmetry

We first illustrate the potential advantages of pulse-based QML models through a four-qubit system. In the gate-based data re-uploading model shown in Fig. 1(a), the input $\mathbf{x} = (x_1, x_2, x_3, x_4)$ is repeatedly uploaded using the encoding circuits $U(\mathbf{x}) = R_z(x_1) \oplus \cdots \oplus R_z(x_4)$. The trainable circuit blocks comprise $R_y(\theta_k)$ ($k = 1, \cdots, n$) rotations about the y-axis, interspersed with the data-uploading circuit blocks. The final learning outcome is inferred by the expectation-value measurement

$$f(\mathbf{x}, \Theta) = \langle \psi(\mathbf{x}, \Theta) | M | \psi(\mathbf{x}, \Theta) \rangle \qquad (1)$$

of a specific observable M, where $|\psi(\mathbf{x}, \Theta)\rangle$ is the output state of the circuit, to approximate multivariable functions by optimizing the parameters $\Theta = \{\theta_1, \cdots, \theta_n\}$.
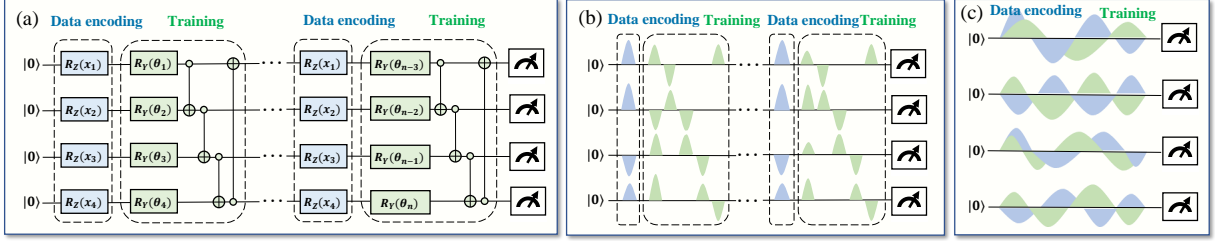
Figure 1: Schematics of (a) a four-qubit gate-based data re-uploading QML model, (b) the pulse-based model compiled from the circuit, and (c) the generalized pulse-based model.

Figure 1(b) illustrates that the physical implementation of the quantum circuit model consistently compiles individual quantum gates into time-varying control pulses on the physical qubits. Let $x_k(t)$ and $\theta_k(t)$ represent the corresponding data-encoding and training control pulses applied to the kth qubit. The QML process can be adjusted by $\Theta = \{\theta_1(t), \cdots, \theta_n(t), \ t \in [0, T]\}$, resulting in a pulse-based model implemented at the physical level. Furthermore, as shown in Fig. 1(c), the pulses can be continuously and simultaneously applied without waiting for one another, allowing for compression to reduce inference time. Such generalized pulse-based model is free from a prior circuit design, featuring more tunable parameters within the finite coherence time, and can achieve greater expressive power than gate-based models [22].

The pulse-based model implemented with an n-qubit quantum device can be characterized as a controlled quantum system:

$$|\dot{\psi}(t; \mathbf{x})\rangle = -i\left[H_{\mathrm{E}}(t, \mathbf{x}) + H_{\mathrm{C}}(t)\right]|\psi(t; \mathbf{x})\rangle, \tag{2}$$

in which the encoding Hamiltonian

$$H_{\mathrm{E}}(t, \mathbf{x}) = \sum_{k=1}^{m} x_k \theta_k(t) H_k \tag{3}$$

encodes the input variable $\mathbf{x} = (x_1, \cdots, x_m) \in \mathcal{X} \subseteq \mathbb{R}^m$ into the dynamical evolution of $|\psi(t; \mathbf{x})\rangle \in \mathbb{C}^{2^n}$. The control Hamiltonian

$$H_{\mathrm{C}}(t) = \sum_{k=m+1}^{m+p} \theta_k(t) H_k \tag{4}$$

is introduced to enhance the expressivity of the pulse-based model. The time-variant functions $\theta_1(t), \cdots, \theta_{m+p}(t)$ are control pulses that

can be trained to fit the dataset. Similar to gate-based models, the output is inferred through the expectation-value measurement

$$f(\mathbf{x}, \Theta) = \langle \psi(T; \mathbf{x})|M|\psi(T; \mathbf{x})\rangle \tag{5}$$

with $\Theta = \{\theta_1(t), \cdots, \theta_{m+p}(t), \ t \in [0, T]\}$. In practice, certain control pulses may be constant or exhibit limited tunability due to hardware constraints.

Let $\mathfrak{g} = \{iH_1, \cdots, iH_{m+p}\}_{LA}$ be the Lie algebra generated by data-encoding and control Hamiltonians in (2), and

$$\mathfrak{g} = \mathfrak{c} \oplus \mathfrak{g}_1 \oplus \cdots \oplus \mathfrak{g}_k$$

be its decomposition as a direct sum of commuting ideals, where $\mathfrak{c}$ is the center of $\mathfrak{g}$ and $\mathfrak{g}_1 \oplus \cdots \oplus \mathfrak{g}_k$ is the semi-simple part. Assume that either the initial state $\rho = |\psi_0\rangle\langle\psi_0|$ or the observable M belongs to the Lie algebra $\mathfrak{g}$ (a relaxed condition can be found in [43]), and the QNN is sufficiently deep (i.e., a sufficiently long time duration T for pulse-based QNN) to establish a 2-design over the Lie group $e^{\mathfrak{g}}$ [41, 42]). The variance of $f(\mathbf{x}, \Theta)$ can be estimated as follows [41, 29]

$$\mathrm{Var}\left[f(\mathbf{x}, \Theta)\right] = \sum_{j=1}^{k} \frac{P_{\mathfrak{g}_j}(\rho)P_{\mathfrak{g}_j}(M)}{\dim(\mathfrak{g}_j)}, \tag{6}$$

where $\dim(\mathfrak{g})$ denotes the dimension of the Lie algebra $\mathfrak{g}$, and

$$P_{\mathfrak{g}}(H) \stackrel{\mathrm{def}}{=} \sum_{j=1}^{\dim(\mathfrak{g})} |\mathrm{Tr}(B_j^\dagger H)|^2$$

denotes the sqaure norm of the orthogonal projection [with respect to the Hilbert-Schmidt inner product $\langle A, B \rangle \stackrel{\mathrm{def}}{=} \mathrm{Tr}(A^\dagger B)$] of H onto $\mathfrak{g}_{\mathbb{C}}$

(the complexification of $\mathfrak{g}$). $\{B_j\}_{j=1}^{\dim(\mathfrak{g})}$ is an orthonormal basis for $\mathfrak{g}$.

The formula (6) indicates that the model becomes untrainable when the underlying control system is fully controllable, because in such case $\dim(\mathfrak{g}) = 4^n$ with $\mathfrak{g} = \mathfrak{su}(2^n)$, yielding exponentially decreasing variance as n increases. Therefore, non-trivial dynamic symmetry must be introduced to constrain the quantum state evolution to a manifold whose dimension does not increase exponentially with n.

3 EXPRESSIVITY OF QML MODELS in presence of dynamical symmetry

The pulse-based model (2) is said to be expressive if, for any function $f_0(\mathbf{x})$ and a specified error threshold $\epsilon > 0$, there exists a suitable control pulse Θ and a scaling factor θ_0 such that the measurement-induced function (5) can approximate the function with the desired precision, i.e., $\|\theta_0 f(\mathbf{x}, \Theta) - f_0(\mathbf{x})\| < \epsilon$.

In a previous study [22], we demonstrated that a pulse-based model is expressive when the underlying system is ensemble controllable (i.e., any $|\psi(T; \mathbf{x})\rangle$ as a function of $\mathbf{x}$ can be realized within a sufficiently long time T). This condition guarantees expressivity for arbitrary selections of the initial state $|\psi_0\rangle$ and the measurement observable M. However, as previously noted, it is overly stringent for trainability.

In the following, we demonstrate that such uncontrollable pulse-based models can be expressive when the initial state and measurement observable are appropriately selected. To derive the required condition, we expand the output function (5) into a polynomial series of $\mathbf{x}$. For convenience, we first rewrite (2) as a Liouville equation:

$$\dot{\rho}(t) = \mathcal{L}(t)\rho(t), \quad \rho(0) = |\psi_0\rangle \langle \psi_0|, \quad (7)$$

where $\rho(t) = |\psi(t)\rangle \langle \psi(t)|$ is the density matrix of the system, and

$$\mathcal{L}(t) = \sum_{j=1}^{m} x_j \theta_j(t) \mathcal{L}_j + \sum_{j=m+1}^{m+p} \theta_j(t) \mathcal{L}_j, \quad (8)$$

with the Liouvillian defined as $\mathcal{L}_j X = -i[H_j, X]$ for $j = 1, \cdots, m+p$.

We then apply the Dyson series expansion (also known as the Fliess expansion in control theory literature [49]):

$$
\begin{aligned}
\rho(t) &= \rho(0) + \int_0^t \mathcal{L}(t_1)\rho(0)\mathrm{d}t_1 \\
&\quad + \int_0^t \mathcal{L}(t_1)\mathrm{d}t_1 \int_0^{t_1} \mathcal{L}(t_2)\rho(0)\mathrm{d}t_2 + \cdots.
\end{aligned}
$$

By substituting (8) and expanding the series into polynomial terms of $x_1, \cdots, x_m$, we obtain the following polynomial expansion:

$$
\begin{aligned}
f(\mathbf{x}, \Theta) &= \mathrm{tr}\,[\rho(T)M] \\
&= \sum_{k_1, \cdots, k_m \geq 0} C_{k_1, \cdots, k_m}(\Theta) x_1^{k_1} \cdots x_m^{k_m},
\end{aligned}
$$

where

$$C_{k_1, \cdots, k_m}(\Theta) = \sum_{n=k_1+\cdots+k_m}^{\infty} \sum_{(j_1, \cdots, j_n) \in \mathbb{J}_{k_1, \cdots, k_m}} c_{j_1 \cdots j_n}(\Theta) \langle \psi_0 | \mathcal{L}_{j_1} \cdots \mathcal{L}_{j_n} M | \psi_0 \rangle. \quad (9)$$

The index set $\mathbb{J}_{k_1, \cdots, k_m}$ comprises tuples $(j_1, \cdots, j_n)$ $(n \geq k_1 + \cdots + k_m)$ wherein each index j in $\{1, \cdots, m\}$ appears k_j times. The coefficients $c_{j_1 \cdots j_n}(\Theta)$ are determined by the control pulses as follows:

$$
\begin{aligned}
c_{j_1 \cdots j_n}(\Theta) = \int_0^T \theta_{j_1}(t_1)\mathrm{d}t_1 \int_0^{t_1} \theta_{j_2}(t_2)\mathrm{d}t_2 \\
\cdots \int_0^{t_{n-1}} \theta_{j_n}(t_n)\mathrm{d}t_n.
\end{aligned} \quad (10)
$$

The polynomial expansion clearly demon-

strates the inherent nonlinearity in the model induced by a continuous-limit data-reuploading mechanism [22]. It is evident that the pulse-based model can approximate any continuous function if the coefficients $\{C_{k_1,\cdots,k_m}(\Theta)\}$ in the polynomial series are fully adjustable by tuning the control pulses $\theta_1(t),\cdots,\theta_{m+p}(t)$. According to (9), the adjustability of these coefficients depends on both the control pulses, through $c_{j_1\cdots j_n}(\Theta)$ terms, and the initial state and observable through $\langle\psi_0|\mathcal{L}_{j_1}\cdots\mathcal{L}_{j_n}M|\psi_0\rangle$ terms.

Ideally, if the coefficients $c_{j_1\cdots j_n}(\Theta)$ are mutually independent and fully adjustable, the model is expressive provided that, for each $(k_1,\cdots,k_m)$, there exist some $(j_1,\cdots,j_n) \in \mathbb{J}_{k_1,\cdots,k_m}$ such that $\langle\psi_0|\mathcal{L}_{j_1}\cdots\mathcal{L}_{j_n}M|\psi_0\rangle \neq 0$. Unfortunately, the mutual independence of $c_{j_1\cdots j_n}(\Theta)$ does not hold, as it can be negated by the counterexample

$$c_{j_1 j_2}(\Theta) + c_{j_2 j_1}(\Theta) = c_{j_1}(\Theta)c_{j_2}(\Theta), \quad \forall\, i,j.$$

Nevertheless, we can derive a necessary condition from this analysis. Observing that the coefficient $C_{k_1\cdots k_m}(\Theta)$ corresponding to the monomial $x_1^{k_1}\cdots x_m^{k_m}$ vanishes when $\langle\psi_0|\mathcal{L}_{j_1}\cdots\mathcal{L}_{j_n}M|\psi_0\rangle = 0$ holds for all $(j_1,\cdots,j_n) \in \mathbb{J}_{k_1,\cdots,k_m}$, we can conclude that the model loses expressivity under these circumstances, regardless of the adjustability of all $c_{j_1\cdots j_n}(\Theta)$. This can be summarized as the following necessary condition for model expressivity.

Theorem 1 *Given a sufficiently long duration T, the pulse-based QML model (2) can approximate any function $f : \mathcal{X} \to \mathbb{R}$ only when $\langle\psi_0|\mathcal{L}_{j_1}\cdots\mathcal{L}_{j_n}M|\psi_0\rangle \neq 0$ for all $(j_1,\cdots,j_n) \in \mathbb{J}_{k_1,\cdots,k_m}\}$ and all $k_1,\cdots,k_m \geq 0$.*

To facilitate the validation of this condition, we denote by

$$\mathcal{S}_{k_1,\cdots,k_m} = \{\mathcal{L}_{j_1}\cdots\mathcal{L}_{j_n}M, \ (j_1,\cdots,j_n) \in \mathbb{J}_{k_1,\cdots,k_m}\}$$

the set of operators associated with the coefficient of $x_1^{k_1}\cdots x_m^{k_m}$ and introduce a recursive procedure for their evaluation. We first define

$$\mathfrak{M}(\mathcal{S}) = \mathrm{span}\{\mathcal{L}_{\alpha_1}\cdots\mathcal{L}_{\alpha_\ell}X, \ X \in \mathcal{S},$$
$$m+1 \leq \alpha_i \leq m+p, \ \ell \in \mathbb{N}\} \quad (11)$$

the submodule generated by the operator set $\mathcal{S}$ with the control Liouvillians. By definition, it is apparent that

$$\mathcal{S}_{0,\cdots,0} = \mathfrak{M}(M)$$

because $\mathbb{J}_{0,\cdots,0}$ contains only tuples $(j_1\cdots,j_n)$ with $m+1 \leq j_k \leq m+p$. Starting from $\mathcal{S}_{0,\cdots,0}$, we can recursively construct $\mathcal{S}_{k_1,\cdots,k_m}$ as follows:

$$\mathcal{S}_{k_1,\cdots,k_i,\cdots,k_m} = \mathfrak{M}\left(\mathcal{L}_i\mathcal{S}_{k_1,\cdots,k_i-1,\cdots,k_m}\right).$$

Theorem 1 provides a method for identifying candidate pulse-based QML models that are both trainable and expressive. Although the sufficiency for expressivity cannot be rigorously proven, subsequent numerical simulations will demonstrate that models meeting this condition tend to be highly expressive. This is attributed to the infinite number of $c_{j_1\cdots j_n}(\Theta)$ terms in (9), which offer considerable flexibility even if they are not mutually independent.

4 Numerical Simulations

In this section, we demonstrate through numerical simulations the expressivity and trainability of pulse-based QML models under selected dynamic symmetries.

Given a training dataset $\{(\mathbf{x}^{(k)}, y^{(k)})\}$ that contain N samples, the model is trained by minimizing the loss function

$$L(\Theta,\theta_0) = N^{-1}\sum_{k=1}^{N}\left\|\theta_0 f(\mathbf{x}^{(k)},\Theta) - y^{(k)}\right\|^2, \quad (12)$$

where $\Theta = \{\theta_1(t),\cdots,\theta_{m+p}(t)\}$. The scaling factor θ_0 is introduced to adapt the function represented by the model to the range of the dataset. Without loss of generality, the domain of $\mathbf{x}$ is always set as $\mathcal{X} = [-1,1]^m$ [22].

In the numerical simulations, the control pulses are chosen in a piecewise-constant form. Each control pulse is divided into K sub-pulses, analogous to the number of layers in gate-based QNN models, with the sub-pulse amplitudes used to parameterize the model. In

all simulations, the sampling period is set to $\Delta t = T/K = 0.1$, and the model is trained by Adam optimizer [50] with a learning rate of 0.05. The simulations are conducted using MATLAB on a computer equipped with two 10-core Xeon CPUs and 208 GB RAM.

4.1 Expressivity of pulse-based models with dynamical symmetry

For the convenience of model description, we adopt the following notation

$$\sigma_\alpha^{(k)} = \mathbb{I}_2 \otimes \cdots \otimes \sigma_\alpha \otimes \cdots \otimes \mathbb{I}_2, \quad \alpha = \text{x}, \text{y}, \text{z},$$

for Pauli operators located on the kth site in an n-qubit system.

We first demonstrate the approximation of univariate functions using a two-qubit model:

$$H[x; \Theta] = x\sigma_\text{z}^{(1)}\sigma_\text{z}^{(2)} + \theta_1(t)\sigma_\text{x}^{(1)} + \theta_2(t)\sigma_\text{x}^{(2)}. \tag{13}$$

The system is not controllable as it possesses a six-dimensional dynamical symmetry algebra:

$$\mathfrak{g} = \{\sigma_\text{z}^{(1)}\sigma_\text{z}^{(2)}, \sigma_\text{x}^{(1)}, \sigma_\text{x}^{(2)}\}_{LA} = \mathfrak{so}(4) \subset \mathfrak{su}(4). \tag{14}$$

We choose the observable $M = \sigma_\text{z}^{(1)}\sigma_\text{z}^{(2)}$ and it can be calculated that

$$\begin{aligned} \mathcal{S}_{2k} &= \{\sigma_\text{z}^{(1)}\sigma_\text{z}^{(2)}, \sigma_\text{y}^{(1)}\sigma_\text{z}^{(2)}, \sigma_\text{z}^{(1)}\sigma_\text{y}^{(2)}, \sigma_\text{y}^{(1)}\sigma_\text{y}^{(2)}\}, \\ \mathcal{S}_{2k+1} &= \{\sigma_\text{x}^{(1)}, \sigma_\text{x}^{(2)}\}, \quad k = 0, 1, 2, \cdots. \end{aligned}$$

According to Theorem 1, if the system is initialized in the state $|\psi_0\rangle = |0\rangle \otimes |0\rangle$, as is typically done, all odd power terms of x will vanish because $\langle\psi_0| \mathcal{S}_{2k+1} |\psi_0\rangle = \{0\}$ for all $k \in \mathbb{N}$. This implies that such a model can only approximate even functions. However, if the initial state is altered to $|\psi_0\rangle = \left(\frac{2}{\sqrt{5}}|0\rangle + \frac{1}{\sqrt{5}}|1\rangle\right) \otimes |0\rangle$, one can verify that $\langle\psi_0| \mathcal{S}_k |\psi_0\rangle \neq \{0\}$ holds for all $k \in \mathbb{N}$, suggesting that the model has the potential to approximate any univariate function.

To validate the above prediction, we apply the model (13) to approximate the following randomly selected target function:

$$\begin{aligned} f_0(x) &= 2x + 3x^2 + x^3 + 10x^6 \\ &+ 8x^7 - 3x^9 + 5x^{10} - 13x^{12}. \end{aligned} \tag{15}$$
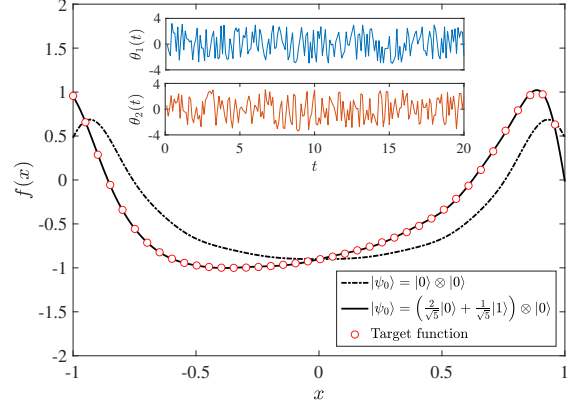
Figure 2: The approximation of the polynomial function (15) using the two-qubit pulse-based model (13) under $\mathfrak{so}(4)$ dynamic symmetry. The inset figure displays the trained control pulses.

from which 200 points are evenly sampled across $\mathcal{X} = [-1, 1]$ to train the model with pulse duration $T = 20$ (corresponding to $K = 200$). The simulation results presented in Fig. 2 indicate that the trained quantum machine learning (QML) model accurately fit the target function when $|\psi_0\rangle = \left(\frac{2}{\sqrt{5}}|0\rangle + \frac{1}{\sqrt{5}}|1\rangle\right) \otimes |0\rangle$. However, when the initial state is $|\psi_0\rangle = |0\rangle \otimes |0\rangle$, the model can only approximate the even part of $f_0(x)$ due to the violation of the necessary condition in Theorem 1.

We also test the fitting of other randomly selected functions, which can all be approximated by the model, provided that the pulse duration is sufficiently long. The required pulse durations tend to be longer when the target function exhibits greater curvature or includes many higher-order power terms.

We further examine the approximation capability of pulse-based models for more complex bivariate functions using the following Hamiltonian:

$$\begin{aligned} H[\mathbf{x}; \Theta] =& x_1\theta_1(t)\sigma_\text{y}^{(1)}\sigma_\text{y}^{(2)} + x_2\theta_2(t)\sigma_\text{z}^{(1)}\sigma_\text{z}^{(2)} \\ &+ \theta_3(t)\sigma_\text{x}^{(1)} + \theta_4(t)\sigma_\text{x}^{(2)}, \end{aligned} \tag{16}$$

which is similar to (13) with an additional Hamiltonian encoding $\sigma_\text{y}^{(1)}\sigma_\text{y}^{(2)}$, and the observable is chosen as $M = \sigma_\text{z}^{(1)} + \sigma_\text{z}^{(2)}$. This model

6

also exhibits $\mathfrak{so}(4)$ dynamic symmetry, and it can be computed that

$$\mathcal{S}_{k_1,k_2} = \{\sigma_y^{(1)}, \sigma_y^{(2)}, \sigma_z^{(1)}, \sigma_z^{(2)}\} \qquad (17)$$

for all cases where $k_1 + k_2$ is even, and

$$\mathcal{S}_{k_1,k_2} = \{\sigma_x^{(1)}\sigma_y^{(2)}, \sigma_y^{(1)}\sigma_x^{(2)}, \sigma_x^{(1)}\sigma_z^{(2)}, \sigma_z^{(1)}\sigma_x^{(2)}\} \qquad (18)$$

for all cases where $k_1 + k_2$ is odd. Accordingly, the initial state is designated as $|\psi_0\rangle = \frac{1}{\sqrt{2}}|0\rangle \otimes (|0\rangle + |1\rangle)$, which can be verified to satisfy the necessary condition in Theorem 1.

In the simulation, the target function is selected as

$$f_0(x_1, x_2) = (x_1^2 + x_2 - 3)^2 + (x_1 + x_2^2 - 1)^2 \quad (19)$$

with $50 \times 50 = 2500$ data points evenly sampled across the domain $\mathcal{X} = [-1, 1] \times [-1, 1]$ and the pulse duration T increased from 0.5 to 4.

For comparison, we train two pulse-based models. In the first case, we set the control pulses $\theta_1(t) = \theta_2(t) \equiv 1$, which considerably limits the tunability of the coefficients $C_{k_1 k_2}(\Theta)$. As illustrated in Fig. 3(a), the fitting progressively aligns with the surface of the target bivariate function as T increases; however, the precision remains limited no matter how T is prolonged. In the second case, we allow $\theta_1(t)$ and $\theta_2(t)$ to vary to enhance the tunability of coefficients $C_{k_1 k_2}(\Theta)$, thereby releasing more expressivity compared to the first case. The fitting results in Fig. 3(b) validate this expectation, as it nearly perfectly matches the target surface when $T = 4$, with a fitting error of $L(\Theta) \leq 10^{-3}$.

4.2 The balance between expressivity and trainability

The simulations above demonstrate that pulse-based models can be expressive when uncontrollable due to dynamic symmetry. This establishes a framework for the design of large-scale pulse-based QML models that are both expressive and trainable. Subsequently, we select four classes of multi-qubit pulse-based models that exhibit various dynamic symmetries.

Model 1. The first model class possesses $\mathfrak{su}(2)$ dynamic symmetry with the following model Hamiltonian:

$$H_1[x; \Theta] = x J_z + \theta_1(t) J_x + \theta_2(t) J_y \quad (20)$$

with two control pulses, where

$$\mathfrak{g} = \{iJ_x, iJ_y, iJ_z\}_{LA} = \mathfrak{su}(2)$$

is the 2^n-dimensional unitary irreducible representation of $\mathfrak{su}(2)$ (see the detailed description in appendix). In this case, the observable is chosen as $M = \frac{2}{2^n - 1} J_z$ and the initial state is chosen as $|\psi_0\rangle = |0\rangle^{\otimes n}$.

Model 2. The second model class possesses $\mathfrak{su}(2)^{\oplus n}$ dynamic symmetry with the following non-interacting n-qubit system:

$$H_2[x; \Theta] = x \sum_{k=1}^{n} \sigma_z^{(k)} + \sum_{k=1}^{n} \left[\theta_x^{(k)}(t)\sigma_x^{(k)} + \theta_y^{(k)}(t)\sigma_y^{(k)} \right] \quad (21)$$

with $2n$ control pulses. The observable is selected as $M = \frac{1}{n} \sum_{k=1}^{n} \sigma_z^{(k)}$, and the initial state $|\psi_0\rangle = |0\rangle^{\otimes n}$.

Model 3. The third model class is selected from Ref. [51] that possesses $\mathfrak{so}(n)$ dynamic symmetry. The Hamiltonian of the model is as follows:

$$H_3[x; \Theta] = x\sigma_x^{(1)}\sigma_y^{(2)} + \sum_{k=1}^{n-1} \theta_k(t)\sigma_x^{(k)}\sigma_y^{(k+1)} \quad (22)$$

with $n - 1$ control pulses. The observable $M = \sigma_x^{(n-1)}\sigma_y^{(n)}$ and the initial state $|\psi_0\rangle = \frac{1}{2}|0\rangle^{\otimes(n-2)} \otimes (|0\rangle + |1\rangle) \otimes (|0\rangle + i|1\rangle)$.

Model 4. The fourth model class is a fully controllable model utilizing the following circularly coupled n-qubit system in [22]:

$$H_4[x; \Theta]$$
$$= x \sum_{k=1}^{n} \sigma_z^{(k)} + \sum_{k=1}^{n} \left[\theta_x^{(k)}(t)\sigma_x^{(k)} + \theta_y^{(k)}(t)\sigma_y^{(k)} \right]$$
$$+ \theta_z^{(1)}(t)\sigma_z^{(1)}\sigma_z^{(2)} + \cdots + \theta_z^{(n)}(t)\sigma_z^{(n)}\sigma_z^{(1)} \quad (23)$$

with $3n$ control pulses. The observable is selected as $M = \sigma_z^{(1)}$ and the initial state as $|\psi_0\rangle = |0\rangle^{\otimes n}$.

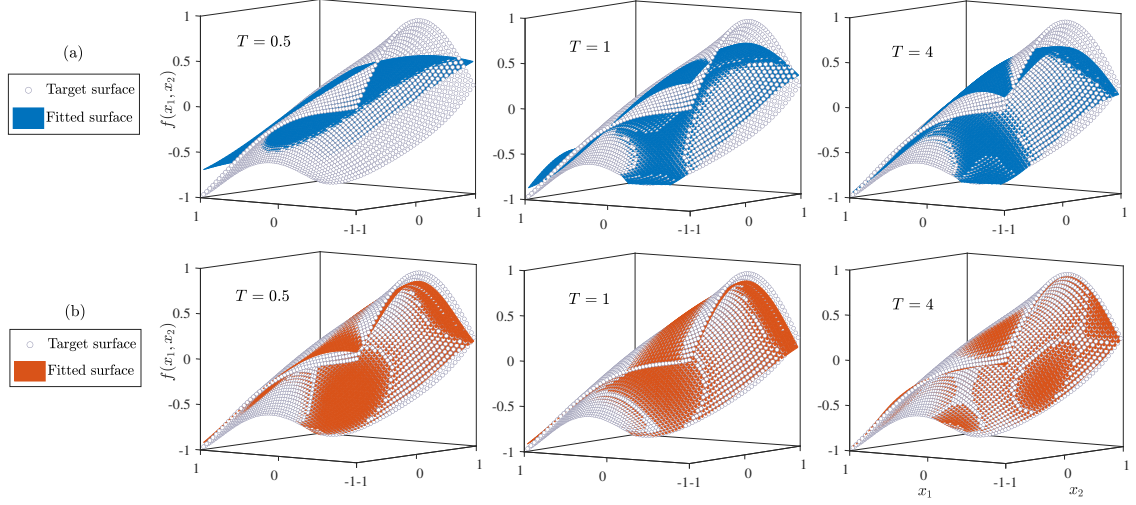The initial states and measurement observables selected in the four models all satisfy the

Figure 3: The approximation results of bivariate function by two-qubit models with (a) $\theta_1(t) = \theta_2(t) = 1$ and (b) $\theta_1(t)$ and $\theta_2(t)$ being freely tunable.

necessary condition in Theorem 1 for expressivity. In addition, the observables are selected from the associated Lie algebra $\mathfrak{g}$ for the sake of trainability [41]. The theoretical variance of the measurement output (5) is presented in Tab. 1 (see the appendix for detailed calculations), which indicates that the variance is inversely proportional to the dimension of the dynamic Lie algebra $\mathfrak{g}$.

During the numerical simulations, these models were trained to fit the univariate function (15). Due to the limitation of computational resource, we use up to six qubits. As can be seen in the inset figure of Fig. 4(a), each model can approximate the target function with arbitrarily small error when the pulse duration T is sufficiently extended. This indicates that the model expressivity grows with T, and thus provides a measure to quantify the degree of expressivity. Here, we adopt the minimal pulse duration required for the training loss to fall below 10^{-3} to evaluate the expressivity (see the inset for illustration).

Based on this measure, the simulation results in Fig. 4(a) compare the variation of expressivity with respect to system size across the four model classes. It is observed that, except the special case of $\mathfrak{su}(2)$ whose dimensionality is constant, the expressivity can be enhanced by increasing the number of qubits.

Furthermore, when the number of qubits is sufficiently large, expressive power increases in the order of $\mathfrak{su}(2)$, $\mathfrak{su}(2)^{\otimes n}$, $\mathfrak{so}(n)$, and $\mathfrak{su}(2^n)$, implying that expressivity can be improved by enlarging the dynamical symmetry Lie algebra.

Regarding the trainability of the models, we estimate the variance of the loss function $L(\Theta)$ in the numerical simulation. Note that the variance of $L(\Theta)$ is different from $\mathrm{Var}[f(\mathbf{x}, \Theta)]$ listed in Table 1 as $L(\Theta)$ is a quadratic function of $f(\mathbf{x}, \Theta)$], and an analytic formula is unavailable. Therefore, we randomly pick 1000 sets of control pulses to numerically evaluate $L(\Theta)$ and its variance. Since the variance is also dependent on the pulse duration T, we make T sufficiently long so that the estimated variance gradually converges to a stationary value, corresponding to the condition under which the model approaches a 2-design.

Figure 4(b) illustrates the relation between the stationary variance and the number of qubits. Consistent with the theoretical analysis in Tab. 1, the variance related to $\mathfrak{su}(2^n)$ exhibits an exponential decline as the number of qubits n increases, indicating the presence of a barren plateau. In contrast, the variance associated with the $\mathfrak{su}(2)$ symmetry remains constant owing to its constant dimensionality, while it decreases at a polynomial rate for the

Table 1: The symmetry Lie algebra, dimension and the variance of the inference output (5) for each model.

Model	$\mathfrak{g}$	$\dim(\mathfrak{g})$	$\mathrm{Var}\left[f(\mathbf{x},\Theta)\right]$
1	$\mathfrak{su}(2)$	3	$\frac{1}{3}$
2	$\mathfrak{su}(2)^{\oplus n}$	$3n$	$\frac{1}{3n}$
3	$\mathfrak{so}(n)$	$\frac{n(n-1)}{2}$	$\frac{2}{n(n-1)}$
4	$\mathfrak{su}(2^n)$	$4^n - 1$	$\frac{1}{2^n+1}$

$\mathfrak{su}(2)^{\otimes n}$ and $\mathfrak{so}(n)$ symmetries.

These observations suggest that barren plateaus can be effectively avoided by restricting the dynamical evolution to sub-manifolds within the quantum state Hilbert space through engineered dynamic symmetry, thereby achieving a good balance between expressivity and trainability. It is noted that the overall expressivity and trainability are highly dependent on the selection of the Hamilton structure, the initial state and the observable. For instance, the expressivity of the larger $\mathfrak{so}(n)$ models is inferior to that of the smaller $\mathfrak{su}(2)^{\otimes n}$ models when the number of qubits is small, as the latter has more tunable control pulses. Nonetheless, their rates of decrease align with predictions, indicating that $\mathfrak{so}(n)$ models will become more expressive than $\mathfrak{su}(2)^{\otimes n}$ models when n is sufficiently large.

5 CONCLUSION AND OUTLOOK

In conclusion, we established a comprehensive framework for designing practical pulse-based QML models that are both expressive and trainable. The design incorporates Dyson polynomial-series expansion alongside existing Lie algebraic theories related to the barren plateau phenomenon in quantum systems exhibiting dynamic symmetry. Theoretical analysis and numerical simulations demonstrate
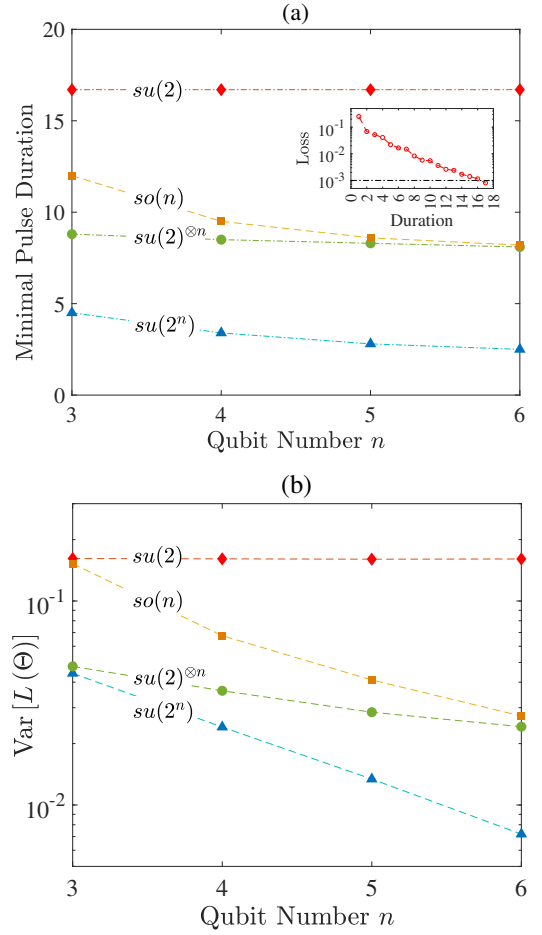

Figure 4: The comparison of expressivity and trainability between model classes under $\mathfrak{su}(2)$, $\mathfrak{su}(2)^{\otimes n}$, $\mathfrak{so}(n)$ and $\mathfrak{su}(2^n)$ dynamic symmetries: (a) The expressivity (evaluated by the minimal pulse duration when the training loss reaches 10^{-3}) versus qubit number for each example . (b) The sample variance of loss function versus qubit number for each example. The inset shows how the minimal pulse duration is obtained. (20).

the potential to leverage dynamic symmetry to construct expressive and trainable pulse-based models suitable for hardware-efficient deployment on NISQ devices.

It remains an open question whether the proposed necessary condition is sufficient for the expressivity of QML models with dynamic symmetry. Simulation results indicate that complete expressivity is not always attainable for models that satisfy this condition, particularly when control pulses are constrained. We conjecture that sufficiency is achieved when all control pulses are unrestricted and the pulse duration is sufficiently long, but this requires verification in the future.

We also note that, even if the pulse-based models are expressive and trainable, the loss landscape may contain undesirable local traps induced by dynamic symmetry [52], which can attract the training process to suboptimal models. Although this issue is rarely encountered in our simulations, the possibility remains, and thus the training algorithm needs to be carefully designed.

Besides the trade-off between model expressivity and trainability, an important issue for future investigation is their trade-off between model generalizability, which pertains to the model's performance on unseen data. The overall balance among these three attributes holds significant practical importance and will be the focus of subsequent studies.

References

[1] Frank Arute, Kunal Arya, Ryan Babbush, Dave Bacon, Joseph C Bardin, Rami Barends, Rupak Biswas, Sergio Boixo, Fernando GSL Brandao, David A Buell, et al. "Quantum supremacy using a programmable superconducting processor". Nature **574**, 505–510 (2019).

[2] Han-Sen Zhong, Hui Wang, Yu-Hao Deng, Ming-Cheng Chen, Li-Chao Peng, Yi-Han Luo, Jian Qin, Dian Wu, Xing Ding, Yi Hu, et al. "Quantum computational advantage using photons". Science **370**, 1460–1463 (2020).

[3] Qingling Zhu, Sirui Cao, Fusheng Chen, Ming-Cheng Chen, Xiawei Chen, Tung-Hsun Chung, Hui Deng, Yajie Du, Daojin Fan, Ming Gong, et al. "Quantum computational advantage via 60-qubit 24-cycle random circuit sampling". Science bulletin **67**, 240–245 (2022).

[4] Hsin-Yuan Huang, Michael Broughton, Jordan Cotler, Sitan Chen, Jerry Li, Masoud Mohseni, Hartmut Neven, Ryan Babbush, Richard Kueng, John Preskill, et al. "Quantum advantage in learning from experiments". Science **376**, 1182–1186 (2022).

[5] Suguru Endo, Zhenyu Cai, Simon C Benjamin, and Xiao Yuan. "Hybrid quantum-classical algorithms and quantum error mitigation". Journal of the Physical Society of Japan **90**, 032001 (2021).

[6] Adam Callison and Nicholas Chancellor. "Hybrid quantum-classical algorithms in the noisy intermediate-scale quantum era and beyond". Physical Review A **106**, 010101 (2022).

[7] Edward Farhi and Hartmut Neven. "Classification with quantum neural networks on near term processors" (2018). arXiv:1802.06002.

[8] Jarrod R McClean, Sergio Boixo, Vadim N Smelyanskiy, Ryan Babbush, and Hartmut Neven. "Barren plateaus in quantum neural network training landscapes". Nature communications **9**, 4812 (2018).

[9] Re-Bing Wu, Xi Cao, Pinchen Xie, and Yu-xi Liu. "End-to-end quantum machine learning implemented with controlled quantum dynamics". Physical Review Applied **14**, 064020 (2020).

[10] Alicia B Magann, Christian Arenz, Matthew D Grace, Tak-San Ho, Robert L Kosut, Jarrod R McClean, Herschel A Rabitz, and Mohan Sarovar. "From pulses to circuits and back again: A quantum optimal control perspective on variational quantum algorithms". PRX Quantum **2**, 010101 (2021).

[11] Alexandre Choquette, Agustin Di Paolo, Panagiotis Kl Barkoutsos, David Sénéchal, Ivano Tavernelli, and Alexandre Blais. "Quantum-optimal-control-inspired ansatz for variational quantum algorithms". Physical Review Research **3**, 023092 (2021).

[12] Oinam Romesh Meitei, Bryan T Gard, George S Barron, David P Pappas, Sophia E Economou, Edwin Barnes, and Nicholas J Mayhall. "Gate-free state preparation for fast variational quantum eigensolver simulations". npj Quantum Information **7**, 155 (2021).

[13] Dekel Meirom and Steven H Frankel. "Pansatz: Pulse-based ansatz for variational quantum algorithms". Frontiers in Quantum Science and Technology **2**, 1273581 (2023).

[14] Zhiding Liang, Hanrui Wang, Jinglei Cheng, Yongshan Ding, Hang Ren, Zhengqi Gao, Zhirui Hu, Duane S Boning, Xuehai Qian, Song Han, et al. "Variational quantum pulse learning". In 2022 IEEE International Conference on Quantum Computing and Engineering (QCE). Pages 556–565. IEEE (2022).

[15] Robert De Keijzer, Oliver Tse, and Servaas Kokkelmans. "Pulse based variational quantum optimal control for hybrid quantum computing". Quantum **7**, 908 (2023).

[16] Zhiding Liang, Jinglei Cheng, Hang Ren, Hanrui Wang, Fei Hua, Zhixin Song, Yongshan Ding, Frederic T Chong, Song Han, Xuehai Qian, et al. "NAPA: intermediate-level variational native-pulse ansatz for variational quantum algorithms". IEEE Transactions on Computer-Aided Design of Integrated Circuits and Systems (2024).

[17] Xiaoxuan Pan, Xi Cao, Weiting Wang, Ziyue Hua, Weizhou Cai, Xuegang Li, Haiyan Wang, Jiaqi Hu, Yipu Song, Dong-Ling Deng, et al. "Experimental quantum end-to-end learning on a super-conducting processor". npj Quantum Information **9**, 18 (2023).

[18] André Melo, Nathan Earnest-Noble, and Francesco Tacchino. "Pulse-efficient quantum machine learning". Quantum **7**, 1130 (2023).

[19] Mohannad M Ibrahim, Hamed Mohammadbagherpoor, Cynthia Rios, Nicholas T Bronn, and Gregory T Byrd. "Evaluation of parameterized quantum circuits with cross-resonance pulse-driven entanglers". IEEE Transactions on Quantum Engineering **3**, 1–13 (2022).

[20] Daniel J Egger, Chiara Capecci, Bibek Pokharel, Panagiotis Kl Barkoutsos, Laurin E Fischer, Leonardo Guidoni, and Ivano Tavernelli. "Pulse variational quantum eigensolver on cross-resonance-based hardware". Physical Review Research **5**, 033159 (2023).

[21] Zhiding Liang, Jinglei Cheng, Zhixin Song, Hang Ren, Rui Yang, Kecheng Liu, Peter Kogge, Tongyang Li, Yongshan Ding, and Yiyu Shi. "Towards advantages of parameterized quantum pulses" (2024). arXiv:2304.09253.

[22] Han-Xiao Tao, Jiaqi Hu, and Re-Bing Wu. "Unleashing the expressive power of pulse-based quantum neural networks" (2024). arXiv:2402.02880.

[23] Vojtěch Havlíček, Antonio D Córcoles, Kristan Temme, Aram W Harrow, Abhinav Kandala, Jerry M Chow, and Jay M Gambetta. "Supervised learning with quantum-enhanced feature spaces". Nature **567**, 209–212 (2019).

[24] Maria Schuld and Nathan Killoran. "Quantum machine learning in feature hilbert spaces". Physical review letters **122**, 040504 (2019).

[25] Maria Schuld. "Supervised quantum machine learning models are kernel methods" (2021). arXiv:2101.11020.

[26] Jonas Jäger and Roman V Krems. "Universal expressiveness of variational quantum classifiers and quantum kernels for

support vector machines". Nature Communications **14**, 576 (2023).

[27] Seth Lloyd. "Almost any quantum logic gate is universal". Physical Review Letters **75**, 346–349 (1995).

[28] Martin Larocca, Piotr Czarnik, Kunal Sharma, Gopikrishnan Muraleedharan, Patrick J Coles, and Marco Cerezo. "Diagnosing barren plateaus with tools from quantum optimal control". Quantum **6**, 824 (2022).

[29] Martin Larocca, Supanut Thanasilp, Samson Wang, Kunal Sharma, Jacob Biamonte, Patrick J Coles, Lukasz Cincio, Jarrod R McClean, Zoë Holmes, and Marco Cerezo. "Barren plateaus in variational quantum computing". Nature Reviews PhysicsPages 1–16 (2025).

[30] Andrew Arrasmith, Zoë Holmes, Marco Cerezo, and Patrick J Coles. "Equivalence of quantum barren plateaus to cost concentration and narrow gorges". Quantum Science and Technology **7**, 045015 (2022).

[31] Qiang Miao and Thomas Barthel. "Equivalence of cost concentration and gradient vanishing for quantum circuits: an elementary proof in the riemannian formulation". Quantum Science and Technology **9**, 045039 (2024).

[32] Leonardo Banchi, Daniel Burgarth, and Michael J Kastoryano. "Driven quantum dynamics: Will it blend?". Physical Review X **7**, 041015 (2017).

[33] Marco Cerezo, Akira Sone, Tyler Volkoff, Lukasz Cincio, and Patrick J Coles. "Cost function dependent barren plateaus in shallow parametrized quantum circuits". Nature Communications **12**, 1791 (2021).

[34] Samson Wang, Enrico Fontana, Marco Cerezo, Kunal Sharma, Akira Sone, Lukasz Cincio, and Patrick J Coles. "Noise-induced barren plateaus in variational quantum algorithms". Nature Communications **12**, 6961 (2021).

[35] Andrew Arrasmith, Marco Cerezo, Piotr Czarnik, Lukasz Cincio, and Patrick J

Coles. "Effect of barren plateaus on gradient-free optimization". Quantum **5**, 558 (2021).

[36] Marco Cerezo and Patrick J Coles. "Higher order derivatives of quantum neural networks with barren plateaus". Quantum Science and Technology **6**, 035006 (2021).

[37] Zoë Holmes, Andrew Arrasmith, Bin Yan, Patrick J Coles, Andreas Albrecht, and Andrew T Sornborger. "Barren plateaus preclude learning scramblers". Physical Review Letters **126**, 190501 (2021).

[38] Kunal Sharma, Marco Cerezo, Lukasz Cincio, and Patrick J Coles. "Trainability of dissipative perceptron-based quantum neural networks". Physical Review Letters **128**, 180505 (2022).

[39] Zoë Holmes, Kunal Sharma, Marco Cerezo, and Patrick J Coles. "Connecting ansatz expressibility to gradient magnitudes and barren plateaus". PRX Quantum **3**, 010313 (2022).

[40] Lucas Friedrich and Jonas Maziero. "Quantum neural network cost function concentration dependency on the parametrization expressivity". Scientific Reports **13**, 9978 (2023).

[41] Michael Ragone, Bojko N Bakalov, Frédéric Sauvage, Alexander F Kemper, Carlos Ortiz Marrero, Martín Larocca, and M Cerezo. "A Lie algebraic theory of barren plateaus for deep parameterized quantum circuits". Nature Communications **15**, 7172 (2024).

[42] Enrico Fontana, Dylan Herman, Shouvanik Chakrabarti, Niraj Kumar, Romina Yalovetzky, Jamie Heredge, Shree Hari Sureshbabu, and Marco Pistoia. "Characterizing barren plateaus in quantum ansätze with the adjoint representation". Nature Communications **15**, 7171 (2024).

[43] N. L. Diaz, Diego García-Martín, Sujay Kazi, Martin Larocca, and M. Cerezo. "Showcasing a barren plateau theory be-

yond the dynamical lie algebra" (2023). arXiv:2310.11505.

[44] Francisco Javier Gil Vidal and Dirk Oliver Theis. "Input redundancy for parameterized quantum circuits". Frontiers in Physics **8**, 297 (2020).

[45] Takahiro Goto, Quoc Hoan Tran, and Kohei Nakajima. "Universal approximation property of quantum machine learning models in quantum-enhanced feature spaces". Physical Review Letters **127**, 090506 (2021).

[46] Adrián Pérez-Salinas, David López-Núñez, Artur García-Sáez, Pol Forn-Díaz, and José I Latorre. "One qubit as a universal approximant". Physical Review A **104**, 012405 (2021).

[47] Maria Schuld, Ryan Sweke, and Johannes Jakob Meyer. "Effect of data encoding on the expressive power of variational quantum-machine-learning models". Physical Review A **103**, 032430 (2021).

[48] Zhan Yu, Hongshun Yao, Mujin Li, and Xin Wang. "Power and limitations of single-qubit native quantum neural networks". Advances in Neural Information Processing Systems **35**, 27810–27823 (2022). url: https://proceedings.neurips.cc/paper_files/paper/2022/file/b250de41980b58d34d6aadc3f4aedd4c-Paper-Confe pdf.

[49] Alberto Isidori. "Nonlinear control systems". Springer Science & Business Media. (1995).

[50] Diederik P. Kingma and Jimmy Ba. "Adam: A method for stochastic optimization" (2017). arXiv:1412.6980.

[51] Roeland Wiersema, Efekan Kökcü, Alexander F Kemper, and Bojko N Bakalov. "Classification of dynamical lie algebras of 2-local spin systems on linear, circular and fully connected topologies". npj Quantum Information **10**, 110 (2024).

[52] Re-Bing Wu, Michael A. Hsieh, and Herschel Rabitz. "Role of controllability in optimizing quantum dynamics". Phys. Rev. A **83**, 062306 (2011).

A Validation of expressivity and variance calculation for the four examples

A.1 Model 1

The Hamiltonian of the model is as follows:

$$H_1[x; \Theta] = x J_z + \theta_1(t) J_x + \theta_2(t) J_y, \tag{24}$$

where $\mathfrak{g} = \{i J_x, i J_y, i J_z\}_{LA} = \mathfrak{su}(2)$ is the 2^n-dimensional unitary irreducible representation of $\mathfrak{su}(2)$. Let $J_\pm = J_x \pm i J_y$ be the raising and lowering operators, and

$$\left\{ |s\rangle \mid s = -\frac{d-1}{2}, -\frac{d-3}{2}, \ldots, \frac{d-3}{2}, \frac{d-1}{2} \right\}$$

be the basis states. Under the basis state, we have

$$
\begin{aligned}
J_z |s\rangle &= s|s\rangle, \\
J_\pm |s\rangle &= \sqrt{\left(\frac{d-1}{2} \mp s\right)\left(\frac{d+1}{2} \pm s\right)} |s \pm 1\rangle.
\end{aligned}
$$

Since the maximum and minimum eigenvalues of J_z are $\pm \frac{2^n-1}{2}$, and the range of the target function is chosen to be $[-1, 1]$, we normalize the observable to $M = \frac{2}{2^n-1} J_z$. According to Theorem 1, it is easy to obtain that

$$\mathcal{S}_k = \{J_x, J_y, J_z\}, k \in N.$$

If the initial state $|\psi_0\rangle = |0\rangle^{\otimes n}$, it can be verified that the model satisfies the condition for expressivity.

On the other hand, the model is uncontrollable and $\dim(\mathfrak{g}) = 3$. Using the orthonormal basis

$$\left\{ \frac{i J_x}{\sqrt{\langle J_x, J_x \rangle}}, \frac{i J_y}{\sqrt{\langle J_y, J_y \rangle}}, \frac{i J_z}{\sqrt{\langle J_z, J_z \rangle}} \right\}$$

of the Lie algebra $\mathfrak{su}(2)$, we have

$$
\begin{aligned}
&\mathrm{Var}\left[f(\mathbf{x}, \Theta)\right] \\
&= \frac{1}{3} P_{\mathfrak{g}}(\rho) P_{\mathfrak{g}}(M) \\
&= \frac{1}{3} \left(\frac{2^n-1}{2}\right)^2 \frac{1}{\langle J_z, J_z \rangle} \left(\frac{2}{2^n-1}\right)^2 \langle J_z, J_z \rangle \\
&= \frac{1}{3}.
\end{aligned}
$$

A.2 Model 2

The Hamiltonian of the model is as follows:

$$H_2[x; \Theta] = x \sum_{k=1}^n \sigma_z^{(k)} + \sum_{k=1}^n \left[\theta_x^{(k)}(t) \sigma_x^{(k)} + \theta_y^{(k)}(t) \sigma_y^{(k)} \right]. \tag{25}$$

The Lie algebra generated by this model is $\mathfrak{g} = \mathfrak{g}_1 \oplus \cdots \oplus \mathfrak{g}_n$, where each $\mathfrak{g}_j = \mathfrak{su}(2)$, thus $\dim(\mathfrak{g}) = 3n$. In this case,

$$\mathcal{S}_k = \{\sigma_x^{(i)}, \sigma_y^{(i)}, \sigma_z^{(i)}\}_{1 \le i \le n}, k \in N.$$

We can verify that $\langle \psi_0 | \mathcal{S}_k | \psi_0 \rangle \neq \{0\}$ for all $k \in N$, which meets the condition in Theorem 1.

Given that the orthonormal basis of $\mathfrak{g}_j$ is $i\{2^{-n/2}\sigma_{\mathrm{x}}^{(j)}, 2^{-n/2}\sigma_{\mathrm{y}}^{(j)}, 2^{-n/2}\sigma_{\mathrm{z}}^{(j)}\}$, we find $M_{\mathfrak{g}_j} = \frac{1}{n}\sigma_{\mathrm{z}}^{(j)}$, and $\rho_{\mathfrak{g}_j} = 2^{-n}\sigma_{\mathrm{z}}^{(j)}$ for all j. Then we obtain

$$
\begin{aligned}
\mathrm{Var}\left[f(\mathbf{x}, \Theta)\right] &= \sum_{j=1}^{n} \frac{1}{3} P_{\mathfrak{g}_j}(\rho) P_{\mathfrak{g}_j}(M) \\
&= \sum_{j=1}^{n} \frac{1}{3} \cdot 2^{-n} \cdot \frac{1}{n^2} \cdot 2^n \\
&= \frac{1}{3n}.
\end{aligned}
$$

A.3 Model 3

The Hamiltonian of the model is as follows:

$$
H_3[x; \Theta] = x\sigma_{\mathrm{x}}^{(1)}\sigma_{\mathrm{y}}^{(2)} + \sum_{k=1}^{n-1} \theta_k(t)\sigma_{\mathrm{x}}^{(k)}\sigma_{\mathrm{y}}^{(k+1)}. \tag{26}
$$

We can derive that

$$
\mathcal{S}_k = \{\widehat{\sigma_{\mathrm{x}}^{(i)}\sigma_{\mathrm{y}}^{(j)}}\}_{1 \leq i < j \leq n}, k \in N,
$$

where $\widehat{\sigma_{\mathrm{x}}^{(i)}\sigma_{\mathrm{y}}^{(j)}} = \sigma_{\mathrm{x}}^{(i)}\sigma_{\mathrm{z}}^{(i+1)}\cdots\sigma_{\mathrm{z}}^{(j-1)}\sigma_{\mathrm{y}}^{(j)}$. For the selected initial state $|\psi_0\rangle = |0\rangle^{\otimes(n-2)} \otimes (\frac{1}{\sqrt{2}}|0\rangle + \frac{1}{\sqrt{2}}|1\rangle) \otimes (\frac{1}{\sqrt{2}}|0\rangle + \frac{i}{\sqrt{2}}|1\rangle)$, we can verify that for any $n \geq 3$, this model satisfies the condition in Theorem 1.

As for the trainability of the model, the Lie algebra associated to this model is $\mathfrak{g} = \mathfrak{so}(n)$ that has dimension $\dim(\mathfrak{g}) = \frac{n(n-1)}{2} \in \mathcal{O}(\mathrm{poly}(n))$. Since the orthonormal basis of $\mathfrak{so}(n)$ is

$$
\{i2^{-n/2}\widehat{\sigma_{\mathrm{x}}^{(i)}\sigma_{\mathrm{y}}^{(j)}} \mid 1 \leq i < j \leq n\},
$$

we can easily get $P_{\mathfrak{g}}(M) = 2^n$ and $P_{\mathfrak{g}}(\rho) = 2^{-n}$. Then we have

$$
\begin{aligned}
\mathrm{Var}\left[f(\mathbf{x}, \Theta)\right] &= \frac{2}{n(n-1)} P_{\mathfrak{g}}(\rho) P_{\mathfrak{g}}(M) \\
&= \frac{2}{n(n-1)}.
\end{aligned}
$$

A.4 Model 4

The model can be verified to possess full expressivity according to the criterion proposed in [22] because the control Hamiltonians generate the entire $\mathfrak{su}(2^n)$ Lie algebra.

For the calculation of variance, based on the analysis of [41], we have

$$
P_{\mathfrak{g}}(M) = 2^n, \quad P_{\mathfrak{g}}(\rho) = 1 - \frac{1}{2^n},
$$

which yields

$$
\mathrm{Var}\left[f(\mathbf{x}, \Theta)\right] = \frac{1}{2^n + 1}.
$$